A Study of the Effect of Attenuation Curvature on Molecular Correlation Energies by Introducing an Explicit Cutoff Radius into Two-Electron Integrals†

Anthony D. Dutoi and Martin Head-Gordon*

Department of Chemistry, University of California at Berkeley, and Chemical Sciences Division, Lawrence Berkeley National Laboratory, Berkeley, California 94720

Received: September 20, 2007; In Final Form: November 6, 2007

We present a new attenuator function that can be applied to the Coulomb operator. Similar to the popular erf(ωr) attenuator, the function [erf($\omega(r + r_0)$) + erf($\omega(r - r_0)$)]/2 divides the Coulomb potential into a singular short-range piece and a non-singular long-range piece. In our attenuator, ω controls the sharpness of the short-range/long-range division at r_0. With $r_0 = 0$, this reduces to erf(ωr), but the additional parameter allows more flexible adjustment of the potential, for physical and/or computational reasons. We present some illustrative results for a truncated MP2 method, where mean field effects are handled exactly and correlation is treated locally. This study indicates, somewhat expectedly, that the slope and curvature of the attenuated potential are more important than its value (a trivial constant may always be added to a potential). However, there are some surprising features of the data that suggest what bounds need to be put on the curvature of the attenuated potential in order to achieve reasonable physics. Conveniently, we find that our attenuator form has the ability to preserve the curvature of the Coulomb potential almost exactly at short range, allowing for the truncation of long-range interactions while preserving the local physics very well. The molecular integrals for the resultant operator can be done analytically over Gaussian basis functions, and the extensive algebraic manipulations necessary to evaluate them stably are shown.

1. Introduction

For some time, the electronic-structure community has been pursuing methods that divide computations into short- and long-range components, with the hope that intelligent truncation of the formal degrees of freedom in a model will yield cheaper yet accurate methods. One piece of this puzzle is the Coulomb operator itself, which couples each pair of electrons. The number of repulsion integrals that must be considered scales minimally quadratically with the number of single-particle basis states that electrons can occupy, and the range of this interaction is too long to be truncated naturally. Indeed, as has been noted before,[1] at a millimeter of separation, the value of the electron−electron Coulomb potential is $\sim 10^{-7}$ a.u. This magnitude is around the convergence threshold for many Hartree−Fock (HF) calculations, but a millimeter is an enormous distance by chemical standards.

Chemists understand that one does not need to consider interaction lengths of millimeters for standard ground-state calculations. Screened interactions produce negligible forces at long range, since matter is largely neutral. On account of this, local correlation algorithms are a mainstay of electronic-structure method development.[2−17]

The relevant question is how one may best trim the dead weight from an electronic-structure computation. Generalization of the fast multipole method of Greengard and Rokhlin[18] allows evaluation of the mean-field Coulomb energy in HF and Kohn−Sham calculations in linear-scaling time.[19] However, this applies to static charge distributions, and it will not circumvent needing a quadratic-scaling number of integrals to represent fluctuation forces in a correlated calculation.

To approach the correlation problem, one might desire a method that allows all but a linear-scaling number of integrals to be discarded in the fluctuation potential. At the size regime where energy becomes extensive, the number of relevant integrals should naturally scale linearly, but in light of the previous statement about the magnitude of these integrals before charge screening, it would probably be necessary to apply a thresholding mechanism to realize this computationally, even asymptotically. For realistic calculations we desire control over the speed/accuracy trade-off by being able to adjust the range of an approximate fluctuation potential explicitly.

This integral thresholding needs to be done carefully, however. A raw distance or integral-value criterion would lead to discontinuities in the energetic surface for the nuclear coordinates.[20] The optimal strategy is to cause integrals to go smoothly to zero, more quickly than the natural Coulomb law. Once outside of the truncation region, an efficient distance criterion may be safely applied. To avoid ambiguity concerning rotations of the single particle basis states, this is best done by modifying the Coulomb operator itself, such that the result corresponds to that of a physical system under a well-defined model potential, rather than a haphazardly truncated basis projection of the full potential. Some set of reasonably localized functions will be needed to obtain an advantage, but we should insist that the answer be invariant to this choice.

We let $V^1(r) = 1/r$ be the Coulomb potential in atomic units, and define a pair of attenuating functions $\alpha(r) + \beta(r) = 1$, where α decreases monotonically from unity to zero over the domain $r \in [0,\infty)$. We are most interested in methods using the short-range potential $V^\alpha(r) = \alpha(r)/r$, but evaluation of the necessary integrals for our attenuator will be more compactly discussed in terms of the trivially related long-range potential $V^\beta(r) = \beta(r)/r$.

† Part of the "William A. Lester, Jr., Festschrift".

* Corresponding author. E-mail: t_dutoi@bastille.cchem.berkeley.edu (A.D.D); mhg@cchem.berkeley.edu (M.H.-G).

10.1021/jp0775956 CCC: $40.75
Published on Web 02/09/2008

Much has been written on the topic of attenuated or short-range Coulomb operators. Work by Gill and co-workers in this area has focused on reducing the amount of computational work necessary in electronic-structure calculations, by dividing the Coulomb operator as described above and choosing different means to evaluate the short- and long-range portions.[21−23] They have also made chemical studies of the effects of neglecting the long-range portion of the Coulomb interaction.[1,24] Panas and Snis have used related integrals in constructing adjusted Coulomb metrics to approximate the short-range correlation associated with the Coulomb hole.[25,26] Savin and co-workers have used divisions of the Coulomb operator to explore the physics of electron−electron interaction and exchange, particularly in the context of density functional theory (DFT), and they have developed correction schemes for the present shortcomings of density functionals.[27−33] Work by Hirao and co-workers has been directed toward chemical studies using such a long-range-corrected density functional,[34] and most recently they have applied these ideas to fixing the charge-transfer problem of time-dependent DFT.[35−39] Scuseria and co-workers have also recently studied and assessed long-range-corrected functionals,[40,41] and they have worked to develop and assess efficiently computable functionals that include only short-range exchange.[42−48] Fixing the long-range behavior of density functionals is a growing area of research,[49−52] and while we explore electron correlation via perturbation theory here, we hope that the flexible attenuator presented in this work will be useful for these purposes as well. Such flexibility may also be useful in a density-fitting metric for resolution-of-the-identity integral codes[53] or in the recently proposed modifications to scaled-opposite-spin MP2 methods.[54,55]

To date, almost all spatial divisions of the Coulomb operator have made use of $\alpha(r) = \mathrm{erfc}(\omega r)$, where ω is an adjustable parameter. This is largely due to the fact that the necessary integrals for using this attenuator are trivially related to those for the regular Coulomb potential. This splitting divides the Coulomb potential into a singular short-range component and a smooth long-range background. In terms of local properties, however, erf and erfc do not yield very fine control over the division of the Coulomb operator, and the short-range component never has the curvature of the Coulomb potential for any finite ω.

Gill and co-workers have improved on this splitting by expanding the background as a sum of increasingly broad Gaussians.[56] While each Gaussian adds only a small amount to the computational time, a large number might be necessary to systematically improve the Hamiltonian, and the variation as such is discretized. Our work could be viewed as an extension of their ideas, where we try to improve on this scheme by introducing an explicit cutoff radius r_0 for the Coulomb potential, by allowing $\alpha(r) = \mathrm{terfc}(\omega r,\omega r_0)$ where

$$\mathrm{terf}(x,y) = \frac{1}{2}\left[\mathrm{erf}(x+y) + \mathrm{erf}(x-y)\right] \qquad (1)$$

and terfc = 1 − terf. The terf function is named for "two erfs," and we note that it approaches zero linearly at the origin, meaning that, again, only the short-range potential is singular. The terfc attenuator essentially turns off the Coulomb potential over a domain of size $\sim 1/\omega$ centered at r_0. Sample plots of the functions terf and terfc are given in Figure 1, as well as an example plot of the Coulomb potential split by this attenuator pair.

In Section 2, we study the correlation energetics of the neon atom and dimer within perturbation theory as the parameters in our attenuator are varied. We pay special attention to the case where $r_0\omega = 1/\sqrt{2}$, as this will be shown to minimize the error in the short-range curvature of the attenuated potential. We compare the behavior of this case of the terfc attenuator to results with a comparable erfc attenuator. In Section 3, we derive the necessary expressions for the numerical implementation of the resulting molecular integrals, discussing the stability of evaluation in detail. In Section 4, we summarize our conclusions from this work.

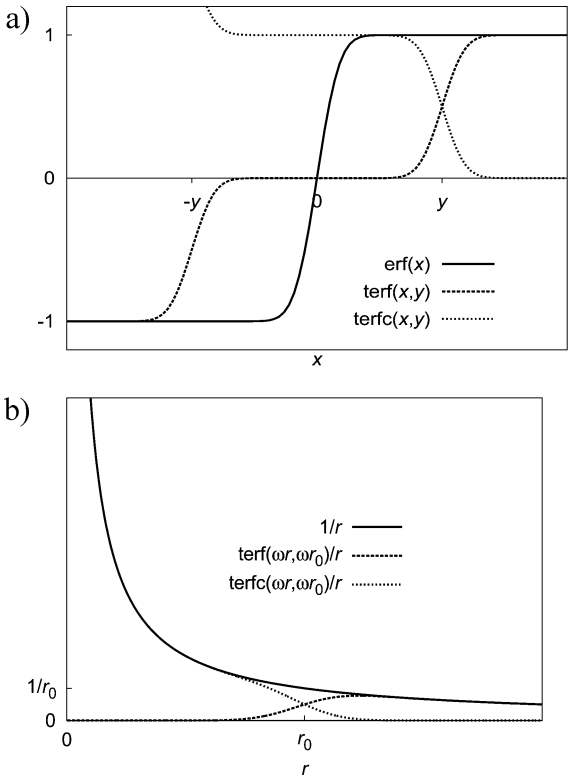

Figure 1. Plots of attenuators and attenuated Coulomb potentials. (a) The functions terf and terfc are plotted, and the shape of erf is shown for reference. (b) A division of the Coulomb potential into short- and long-range components by terfc and terf, respectively ($\omega = 5/r_0$). Increasing ω sharpens the truncation at the cutoff radius of r_0.

2. A Local Møller−Plesset Model

2.1. Method Definition. One can consider a split Hamiltonian in the correlation calculation only, such that long-range effects are handled by the proper Coulomb operator at the HF level. In this way monopole and mean-field multipole induction effects will be properly included in charged or charge-separated systems.

Let $\hat{H}$ be the usual nonrelativistic electronic Hamiltonian and $\hat{F}$ be the converged Fock operator, using the full Coulomb potential. Allow the many-electron Coulomb operator $\hat{V}^1$ to be split into short- and long-range pieces $\hat{V}^\alpha$ and $\hat{V}^\beta$, respectively, such that $\hat{V}^1 = \hat{V}^\alpha + \hat{V}^\beta$. Let $\hat{H}^{\mathrm{Short}}$ be defined by $\hat{H} = \hat{H}^{\mathrm{Short}} + \hat{V}^\beta$, so that $\hat{H}^{\mathrm{Short}}$ includes $\hat{V}^\alpha$ and the kinetic and nuclear-attraction operators. Similarly, let $\hat{F} = \hat{F}^{\mathrm{Short}} + \hat{v}^\beta$, where $\hat{v}^\beta$ is the long-range part of the effective mean-field potential, built using the converged occupied space from the full Coulomb operator.

Now say we want to solve for the ground state of $\hat{H}' = \hat{H}^{\mathrm{Short}} + \sum_x \hat{v}_x^\beta$ (x runs over electron labels) within second-order Møller−Plesset perturbation theory (MP2). The unperturbed Hamiltonian is taken to be $\sum_x \hat{F}_x$, and a Brillouin-like exclusion of single excitations can be derived. This results in an MP2

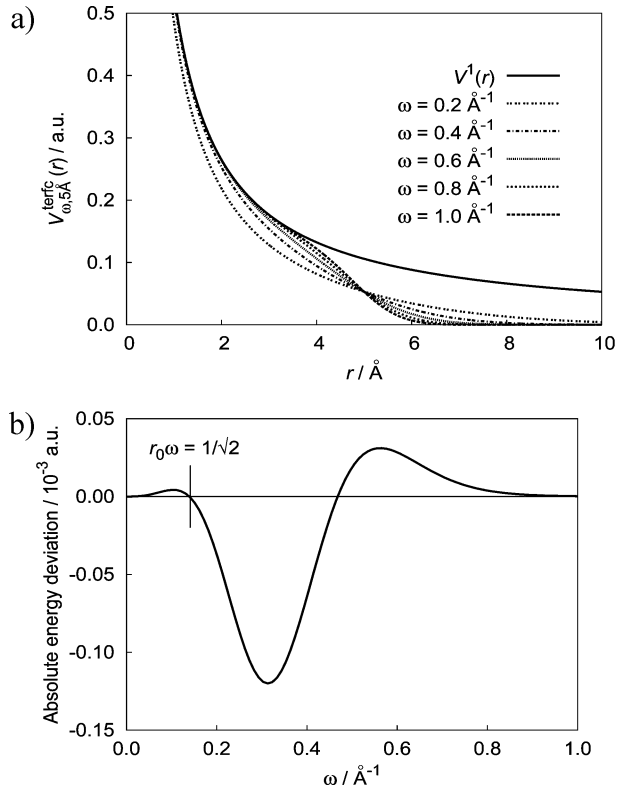

Figure 2. Attenuated Coulomb potentials and resultant atomic correlation energies. (a) Short-range Coulomb potentials with $r_0 = 5$ Å and different values of ω. (b) The MP2/cc-pVDZ energy of a Ne atom, relative to the unattenuated result, for the continuous family of fluctuation potentials generated by varying ω with $r_0 = 5$ Å. The zero of this curve at $\omega = 0.14$ Å^{-1} is meaningful, because the short-range curvature of the Coulomb potential is optimally preserved when $r_0\omega = 1/\sqrt{2}$.

expression where the usual integrals involving occupied orbitals i and j and virtuals a and b are simply replaced by $\langle a|\langle b|\hat{V}^{\alpha}|i\rangle|j\rangle$. We emphasize that, as we explore the behavior of correlation with respect to the parameters in the attenuated potential, the HF reference state in each calculation is obtained with the unattenuated potential, and it is independent of these parameters.

2.2. The Ne Atom. We start by examining the behavior of our attenuated MP2 method on a closed-shell atom, namely neon, using the cc-pVDZ basis set. To simplify the discussion, we first take $r_0 = 5$ Å, which is well larger than the atomic diameter, such that any two points in space that are likely to be occupied by a pair of electrons are separated by less than this distance. Variations in the attenuated Coulomb potential as a function of ω and the resulting deviation of the atomic absolute energy are shown in Figure 2.

Two limits are immediately evident in Figure 2. First, as $\omega \rightarrow \infty$, the cutoff becomes sharper, and since the entire atom lives within a diameter of 5 Å, the full MP2 energy is recovered. Second, as $\omega \rightarrow 0$, the cutoff region becomes extremely broad, and the full MP2 energy is again recovered. There are two intuitively possible consequences as this cutoff region approaches infinitely broad: the first is that the whole short-range potential is attenuated to zero, and the second is that no part of the potential is ever attenuated. It is easy to show that the latter is true, and hence the full MP2 energy is recovered. In the intermediate-ω regimes, the cutoff region is of finite width and extends well inside the 5 Å formal cutoff radius, and the energy of the atom is modified significantly.

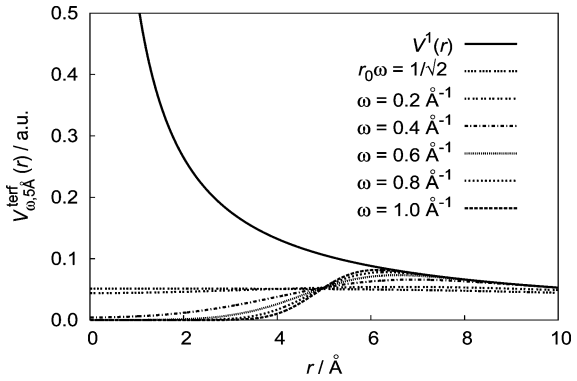

Figure 3. The complement of the attenuated Coulomb potentials in Figure 2a, such that the changes in short-range forces may be illustrated for each ω. A large slope near the cutoff radius here indicates a countering slope in the short-range potential, which produces unphysical forces. Note the flat appearance of these complement curves at the origin as $\omega \rightarrow 0.14$ Å$^{-1} = 1/r_0\sqrt{2}$ (which preserves the short-range forces of the Coulomb operator in the short-range potential). Values of ω that are lower than $1/r_0\sqrt{2}$ give rise to curves that would look like flat lines on the scale of this plot, with the value of the potential approaching zero everywhere as $\omega \rightarrow 0$; in the $\omega \rightarrow 0$ limit, their shape approaches that of the erf-attenuated complement potential (see Figure 6), but with small ω.

Attention should be drawn to one of the other two cases in Figure 2b in which the full MP2 energy is recovered ($\omega = 0.14$ Å^{-1}), which can be shown not to be an accidental cancellation of errors.

First, we briefly remind the reader that there is a gauge invariance in the potential formulation of particle−particle interactions, so that adding an arbitrary constant to a potential does not change particle-number-conserving relative energies, including correlation energies. Therefore, we focus our attention on the slope and curvature of the attenuated V^{α} potential. Since it is rather difficult to see the change in curvature with varied ω, due to the singularity, the complementary V^{β} long-range potentials (deviation of V^{α} from the Coulomb potential) have been plotted in Figure 3 for the same choices of ω as in Figure 2a, with the same r_0. In regions where this long-range potential has a nonzero slope, we can deduce that the corresponding short-range potential (same parameters) has the opposite deviation in its slope from that of the Coulomb potential. This is effectively an additional artifactual force between the electrons (which, at long range, is equal and opposite to the Coulomb force, hence the attenuation).

If we were to attempt to minimize the first derivative of V^{β} over the short-range region, so as to minimize the force deviation of V^{α} over this same region, we might try setting the second derivative of V^{β} to zero at the origin, limiting the expansion at that point to quartic and higher even terms. Thus, we can derive the condition $r_0\omega = 1/\sqrt{2}$ for which the complementary potential V^{β} is as flat as possible near the origin. An example of such a V^{β} potential is shown in Figure 3. One can see that the potential starts flat at a finite value and begins to turn into the Coulomb potential near r_0 (see also Figure 6). Using V^{α} with $r_0\omega = 1/\sqrt{2}$ is reminiscent of a long-standing trick in classical dynamics, in which a potential is truncated, shifted downward, and perhaps smoothed.

2.3. The Ne_2 Dimer. Considering that our primary interest is the forced decay of the correlation interaction with respect to distance, we now turn our attention to Ne_2, which will be studied as a function of nuclear separation, with the same attenuated potentials and basis. No integrals were discarded in the algorithm for which results are presented, but it should be

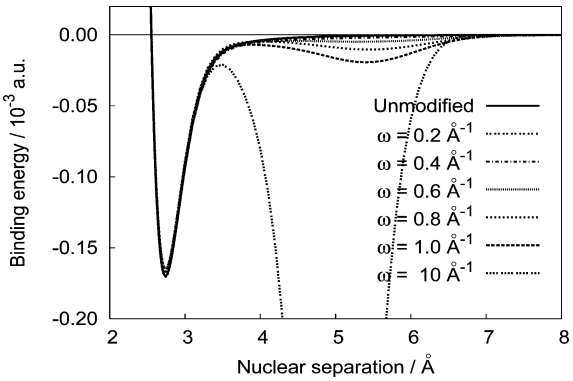

Figure 4. The MP2/cc-pVDZ interaction curves of Ne_2 for the attenuated potentials in Figure 2a ($r_0 = 5$ Å). Each curve is relative to the energy of two Ne atoms with the same fluctuation potential. The extraneous minima are the result of unphysically strong correlations when electrons are separated by a distance of nearly the cutoff radius. The unphysical minima disappear for the lower parameter values.

clear that some integrals could be discarded at larger distances (at least in the atomic basis representation[57]) without affecting the energetic results. Dimer interaction curves are shown in Figure 4 for the set of potentials pictured in Figure 2a.

The most striking feature of the majority of these curves is the unphysical second minimum near 5 Å separation, where the Coulomb interaction was truncated. For very large ω, the depth of this minimum even exceeds that of the physically meaningful binding well, as can be seen for $\omega = 10$ Å^{-1} (which is near the $\omega \rightarrow \infty$ limit for our purposes). This effect is easily explained by looking at the form of the MP2 correction. It is an energetically weighted sum over (the squares of) all possible pairs of occupied−virtual product-distribution interactions. By orthogonality of the occupieds and virtuals, we know that each product distribution generates, at most, a dipolar field. Since the MP2 correction is therefore a sum over dipolar and higher order interactions, the interaction between the two neon atoms would be monotonically decaying (beyond the physical minimum) only if the dominant dipole−dipole interactions are decreasing in strength with distance, which is not the case for some of the V^{α} plotted in Figure 2a.

We again consider the curvature of the attenuated operator. It is an easy numerical exercise to show that the dipole−dipole interaction, which goes as the second derivative of the potential, is monotonically decreasing for our attenuator under the condition that $r_0\omega \leq 2.06987$. Indeed, for the lower two values of ω in Figure 4 ($r_0\omega \leq 2$), there is no extraneous minimum. Furthermore, $1/\sqrt{2} < 2.06987$, so we have no contradiction between conditions we would like to satisfy.

A satisfying interpretation of this is available in terms of forces. If the Coulomb operator is truncated sharply, then near the region of this truncation, the potential energy of the system is lowered a lot by small displacements of the electrons from their mean-field equilibrium; strong forces (large derivatives) lead to strong and energetically significant correlations.

Figure 5 shows how the variation of ω affects the long-range portion of the interaction and the region of the equilibrium minimum. As expected, the long-range interactions decay to zero at a shorter distance than with the unattenuated potential, and the interaction goes more quickly to zero with a more steeply truncated potential. It is encouraging that the curve with $r_0\omega = 1/\sqrt{2}$ tracks the full MP2 curve much more closely than the others at long range in Figure 5a. While we expect further improvement as ω tends to zero (recovering the full Coulomb potential), it is remarkable how much improvement there is

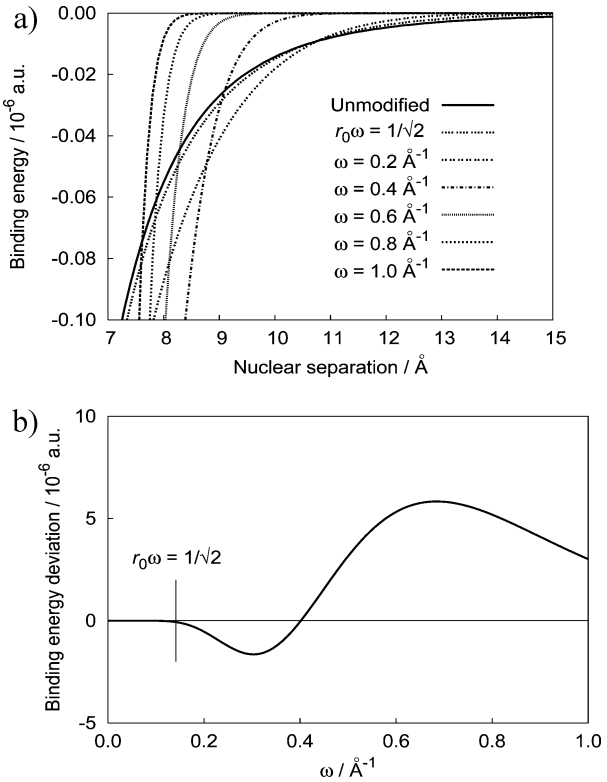

Figure 5. Further examination of the Ne_2 curves in Figure 4. Both sets of results improve as $\omega \rightarrow 0$; however, very good results are obtained with $r_0\omega = 1/\sqrt{2}$, and the finite ω would allow the attenuated potential to be neglected at some radius (dependent on a threshold). (a) Magnified view of the large-separation regime, where steeper quenching of the dispersion interaction with increasing ω can be seen. (b) The deviation of the binding energy from the unattenuated result as a continuous function of ω at a nuclear separation of 2.74 Å (equilibrium for the unattenuated potential).

between the $\omega = 0.2$ Å^{-1} curve and the $\omega = 0.14$ Å^{-1} ($r_0\omega = 1/\sqrt{2}$) curve, considering that their complement potentials look so similar in Figure 3.

Near the equilibrium region in Figure 5b, we again see that, as ω tends toward zero or infinity, the result tends toward the full MP2 result. The main point of difference from Figure 2b for atomic absolute energies (other than the energetic scale of the quantity considered) is that the relative sizes of the small- and large-ω features has changed. This is most easily viewed as a relative exaggeration of the deviation at higher ω for the dimer. As can be seen in Figure 3, as ω is increased, the region of adversely affected curvature is increasingly localized around r_0. Because the dimer does not fit entirely within a diameter of 5Å, the interatomic correlations remain sensitive to this poor curvature at $r \approx r_0 = 5$ Å for all ω, while the intraatomic correlations of Figure 2b begin to fall within a radius where the potential is no longer altered as ω increases. Unlike in the atomic case, the numerically exact full MP2 result is not achieved for the dimer as $\omega \rightarrow \infty$, and the deviation asymptotes to -5×10^{-9} a.u. It is again encouraging that the binding energy is obtained very accurately for all ω smaller than $\sim 1/r_0\sqrt{2}$.

In the foregoing text, it has been shown that, for fixed r_0, the best choice of finite ω seems to be $1/r_0\sqrt{2}$. The computationally advantageous attenuation disappears as $\omega \rightarrow 0$, and patently absurd results are obtained in the $\omega \rightarrow \infty$ extreme. To clean up the notation, the constant $1/\sqrt{2}$ will hereafter be represented symbolically as γ.

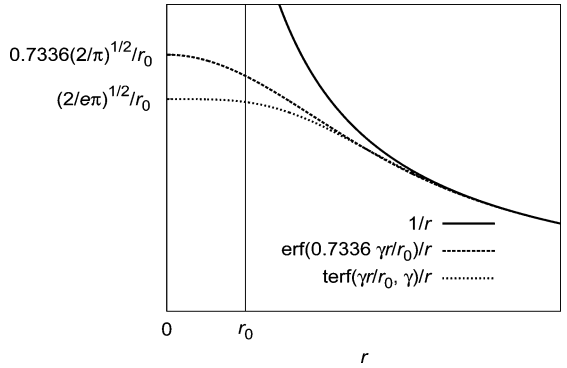

Figure 6. Complements of terfc- ($\omega = \gamma/r_0$) and erfc-attenuated potentials for given r_0, with ω' chosen for best correspondence between them. Given some threshold, these potentials and their derivatives are both the same as the Coulomb potential to within that threshold at about the same distance, such that both of the complement short-range potentials can be considered to have vanished at comparable distances. This comparison looks the same for all values of r_0.

2.4. Comparison with the erfc Attenuator. Now, regarding $\omega = \gamma/r_0$ as a function of r_0 rather than as a separate parameter, we discuss variation of r_0 as well as comparison to the erfc attenuator. Hereafter, ω' will denote the variable parameter in erfc($\omega' r$), and ω retains its meaning for the terfc attenuator. In order to make the comparison of these two attenuators more orderly, we attempt to draw a correspondence between attenuated potentials with a specific value of r_0 in the terfc attenuator ($\omega = \gamma/r_0$) and a corresponding value of ω' in the erfc attenuator. Again, we work with the finite long-range complementary potentials V^β for convenience. If the erf- and terf-attenuated V^β potentials are aligned such that both potentials and their derivatives come within the same threshold of being the same as the Coulomb operator at about the same value of r, then the two corresponding attenuated short-range potentials can be neglected to within the same tolerance at that distance, allowing the distance-based filtering of the same number of integrals for each attenuator in a given calculation.

Because both complement potentials have the general appearance of being concave-up in the outer domain, where they approach Coulombic behavior, and being concave-down in the inner domain, we expect a reasonable correspondence to be drawn if we insist that the potential curves intersect at the inflection point of one or the other attenuated potentials. Arbitrarily, we choose the inflection point of the terf-attenuated potential, which numerically leads to the condition $\omega' = 0.7336\omega = 0.7336\gamma/r_0$. Examples of corresponding erf- and terf-attenuated potentials are shown in Figure 6; since these curves are self-similar under change of r_0 with the corresponding variations in ω and ω', this is a perfectly general example of the kind of correspondence achieved by this condition. (Self-similarity here means that some scaling of the horizontal and vertical axes allow any two such plots with different r_0 to be identically superimposed on one another.) In the outer region, the two curves track each other well for some distance inside the region where they are both very much like the Coulomb operator, but only the terf-attenuated potential has the appearance of being constant for any part of the inner domain (flat out to almost r_0). We can now scan the behavior of the erfc-attenuated short-range potential for all ω' and make a reasonable comparison to the best case of the terfc-attenuated potential with a similar attenuation radius.

The deviation of the attenuated result from the full MP2 result for the absolute energy of the Ne atom is shown in Figure 7a for both corresponding potentials as a function of the effective truncation radius (r_0 of the terf attenuator). In Figure 7b, the same comparison is made for the Ne_2 binding energy.

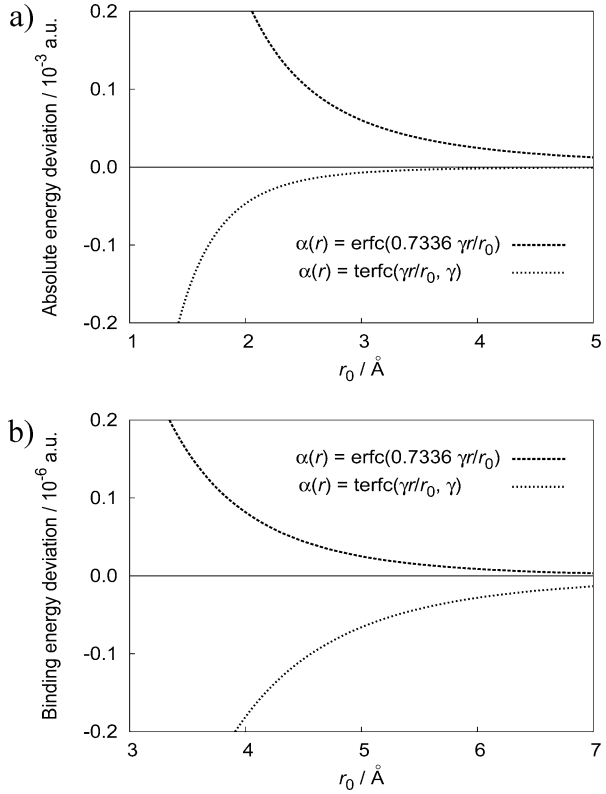

Figure 7. Deviations in MP2/cc-pVDZ energetics for fluctuation potentials V^α, relative to using the unattenuated potential, where α is either the erfc or the terfc attenuator. The attenuators both depend on an effective Coulomb cutoff radius r_0, and the other parameters have been chosen to give good correspondence between the potentials for that r_0. (a) Deviation of the absolute energy of a Ne atom. (b) Deviation of the binding energy of the Ne_2 dimer at a nuclear separation of 2.74 Å (equilibrium for the unattenuated potential).

On account of the better preserved Coulombic curvature of the terfc-attenuated potential at short range, the absolute energy of the atom converges to the full MP2 result more quickly with r_0 than does the result with the erfc attenuator. To be clear, the terfc-attenuated curve in Figure 7a exhibits a minimum of depth -10^{-3} a.u. at around $r_0 = 0.75$ Å, and both attenuators deviate by exactly the negative of the full correlation energy at $r_0 = 0$ (qualitatively similar in Figure 7b).

Figure 7b shows that the result of the erfc-attenuated calculation converges more quickly with r_0 for the well depth. This is counter-intuitive, as we would expect that the same curvature-of-the-potential argument as above would hold for molecules as for atoms, for large enough r_0. The explanation for this seems to lie in some fortuitous cancellation of errors for the erfc-attenuated case, because the absolute energies of both the atom and dimer converge more quickly with the terfc attenuator. Each of the three calculations (the erfc- and terfc-attenuated ones and the unattenuated one) begin with the same HF reference state, and we would certainly expect the interatomic correlations with the terfc attenuator to converge faster to the unattenuated result; however, this small-energy-scale interaction may be obscured by the way that changes in the larger intraatomic correlations contribute to the binding energy for each of these attenuators. We suppose that this is not a general phenomenon, and we also note that the difference in how the two attenuators converge for absolute energies is more dramatic than for the dimer relative energies. As a counter-example, a similar plot is presented for the N_2 molecule in Figure

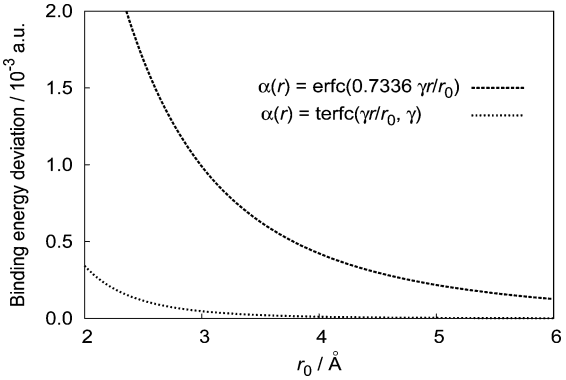

Figure 8. Deviations in the MP2/cc-pVDZ binding energy of N_2 at a nuclear separation of 1.13 Å (equilibrium for the unattenuated potential) for fluctuation potentials V^{α}, relative to using the unattenuated potential, where α is either the erfc or the terfc attenuator. The attenuators both depend on an effective Coulomb cutoff radius r_0, and the other parameters have been chosen to give good correspondence between the potentials for that r_0.

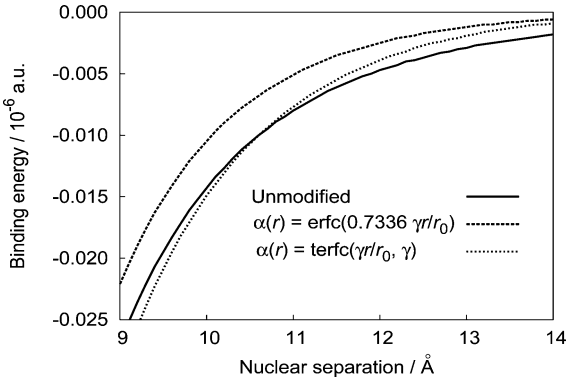

Figure 9. Comparison of the long-range behavior of the MP2/cc-pVDZ Ne_2 interaction for fluctuation potentials V^{α}, where α is either the erfc or the terfc attenuator. The attenuators both have an effective Coulomb cutoff radius of $r_0 = 5$ Å, and the other parameters have been chosen to give good correspondence between the potentials. Comparison of dimer interaction curves for different values of r_0 are qualitatively similar. The roughness of the curves is because these small relative energies are only manifested in the last few printed digits of the absolute energies.

8, where the correlations involved with the bond are much less subtle, and the result with the terfc-attenuated fluctuation potential converges much more quickly.

Finally, we observe the long-range region of the Ne_2 dimer interaction curve for the erfc and terfc attenuators in Figure 9. At the distances shown, changes in intraatomic correlations with nuclear separation should be negligible. The erfc attenuator truncates the dispersion forces in a more gradual fashion, but the curves are separated by less than 5×10^{-9} a.u. in this regime.

3. Integral Calculus

3.1. Repulsion Integrals in General. We now discuss the computation of repulsion integrals with our proposed attenuator. In this work, we will largely follow the development of Gill,[58] with some minor variation in the notation. To compute the particle−particle interaction integral for an arbitrary spherically symmetric interparticle potential V over a quartet of Gaussian s basis functions, the integration can be reduced to a fundamental integral I_{pq}. This integral is the average interaction of two classical, spherical Gaussian distributions under the same potential V; we normalize the distributions here.

$$I_{pq}[V](R) = \int\int \left[\left(\frac{p}{\pi}\right)^{3/2} e^{-p\vec{r}_1^{\,2}}\right] V(|\vec{r}_2 - \vec{r}_1|)\left[\left(\frac{q}{\pi}\right)^{3/2} e^{-q(\vec{r}_2 - R\vec{z})^2}\right] d\vec{r}_1 d\vec{r}_2 \quad (2)$$

The integral has a functional dependence on V and parametric dependences on the exponents p and q, which are related to the exponents of the original basis function quartet. The integral depends most importantly on the distance R between the two distributions, which is related to the original basis function positions and exponents ($\vec{z}$ is a unit vector in an arbitrary direction). We will need derivatives of the fundamental integral with respect to R, in order to compute integrals for higher angular momentum basis functions. During the subsequent steps in building the final primitive shell interaction integrals from this fundamental integral and its derivatives, R is usually handled in terms of a variable T, related to R^2, but these details have been discussed elsewhere, and we shall not repeat them here. Likewise, the handling of the R-dependent prefactor to this integral and all subsequent contractions is not dependent on the choice of V, and so we refer the curious reader to existing literature on conventional Coulomb integrals.[58,59]

I_{pq} can be reduced to a one-dimensional integral in inverse space

$$I_{pq}[V](R) = \frac{4\pi}{R^3}\int_0^{\infty} u\sin(u)\Lambda(u/R)e^{-(1/p+1/q)u^2/4R^2}\,du$$
$$\Lambda(|\vec{k}|) = \frac{1}{8\pi^3}\int V(|\vec{r}|)e^{-i\vec{k}\cdot\vec{r}}\,d\vec{r} \quad (3)$$

Integrating over the angular parts of the interparticle vector for a general attenuated potential $V^{\beta}(r) = \beta(r)/r$ in eq 3, we have

$$\Lambda^{\beta}(k) = \frac{1}{2\pi^2 k}\int_0^{\infty} \sin(kr)\beta(r)\,dr \quad (4)$$

in terms of the attenuating function β. For $\beta(r) = \mathrm{terf}(\omega r,\omega r_0)$, this integrates to

$$\Lambda^{\mathrm{terf}}_{\omega,r_0}(k) = \frac{\cos(kr_0)e^{-k^2/4\omega^2}}{2\pi^2 k^2} \quad (5)$$

where the antisymmetry of terf across r aids in a trick for the integral evaluation (Fourier transformation of the integrands), and we ultimately obtain

$$I_{pq}[V^{\mathrm{terf}}_{\omega,r_0}](R) = \frac{2}{\pi R}\int_0^{\infty} \frac{\cos((r_0/R)u)\,\sin(u)e^{-(1/p+1/q+1/\omega^2)u^2/4R^2}}{u}\,du$$
$$= \frac{1}{R}\,\mathrm{terf}(\varphi R,\varphi r_0) \quad (6)$$

where

$$\varphi = \left(\frac{1}{p} + \frac{1}{q} + \frac{1}{\omega^2}\right)^{-1/2} \quad (7)$$

This integral is done by inserting the trigonometric identity for the multiplied sin and cos functions, giving a form that is familiar from the unattenuated potential.

We now draw attention to two important limits of this potential and the resulting integral. The first limit is $r_0 \rightarrow 0$:

$$V_\omega^{\mathrm{erf}}(r) = V_{\omega,0}^{\mathrm{terf}}(r) = \frac{1}{r}\,\mathrm{erf}(\omega r); \qquad \Lambda_\omega^{\mathrm{erf}}(k) = \frac{\mathrm{e}^{-k^2/4\omega^2}}{2\pi^2 k^2}$$

$$I_{pq}[V_\omega^{\mathrm{erf}}](R) = \frac{1}{R}\,\mathrm{erf}(\varphi R) \tag{8}$$

This result is familiar from literature concerning attenuated Coulomb integrals.[56] The second interesting limit is the unattenuated Coulomb interaction $V^1 = V_{\infty,0}^{\mathrm{terf}}$ obtained by taking the $\omega \rightarrow \infty$ limit of the expressions in eq 8, ultimately resulting in the well-known formula

$$I_{pq}[V^1](R) = \frac{1}{R}\,\mathrm{erf}(\vartheta R); \qquad \vartheta = \left(\frac{1}{p} + \frac{1}{q}\right)^{-1/2} \tag{9}$$

3.2. Fundamental Integral Evaluation. Similar to the known transformation

$$I_{pq}[V^1](R) = \frac{2\vartheta}{\pi^{1/2}}\left[\int_0^1 e^{-Tu^2}\,\mathrm{d}u\right] = \frac{2\vartheta}{\pi^{1/2}}\,F_0(T); \qquad T = (\vartheta R)^2 \tag{10}$$

we can write

$$I_{pq}[V_{\omega,r_0}^{\mathrm{terf}}](R) = \frac{2\varphi}{\pi^{1/2}}\left[\frac{1}{2}\int_{-1}^1 e^{-(S^{1/2}u+s^{1/2})^2}\,\mathrm{d}u\right] = \frac{2\varphi}{\pi^{1/2}}\,G_0(S,s)$$

$$S = (\varphi R)^2; \qquad s = (\varphi r_0)^2 \tag{11}$$

without loss of generality, since the integral is an even function of R and r_0.

For the conventional V^1 integral, it could be viewed as a fortuitous accident that the dependences of F_0 on p and q along with the dependence on R can all be folded together into the single variable T. This means that differentiation with respect to variation in R (for higher angular momenta), as well as interpolation by power series for continuous values of R, p and q, may be handled simultaneously. However, both S and s depend on p and q, and it will be necessary to compute derivatives with respect to s as well, in order to make a two-dimensional interpolation table. Usually, we evaluate F_0 and its mth derivatives with respect to T, known as the F_m (to within a sign convention). Similarly, we are interested in evaluating G_0 and its derivatives with respect to S, the G_m, up to some given m ($m_{\max} = 4l_{\max}$, where $l_{\max}$ is the maximum orbital angular-momentum quantum number for a given basis), where G_m is an abbreviation for $G_m^{(0)}$:

$$G_m^{(n)}(S,s) = \left(-\frac{\partial}{\partial S}\right)^m \left(-\frac{\partial}{\partial s}\right)^n G_0^{(0)}(S,s) \tag{12}$$

Since the expressions for F_0 and G_0 contain erf, there can be no closed form expression for them. In the case of the F_m, however, one can find a decaying series of all positive terms to express each F_m:

$$F_m(T) = \left(-\frac{\partial}{\partial T}\right)^m F_0(T) = \int_0^1 u^{2m}\mathrm{e}^{-Tu^2}\,\mathrm{d}u =$$

$$\mathrm{e}^{-T}(2m-1)!!\sum_{i=0}^{\infty}\frac{(2T)^i}{(2m+2i+1)!!} \tag{13}$$

This allows us to construct the F_m to arbitrary precision at regular intervals to construct a power series interpolation table. In practice, the interpolation table only needs to be constructed out to some cutoff, at which point the asymptotic expression is accurate to within machine precision:

$$\lim_{T\rightarrow\infty} F_m(T) = \frac{\pi^{1/2}(2m-1)!!}{2^{m+1}}\left(\frac{1}{T}\right)^{m+1/2} \tag{14}$$

Unfortunately, the G_m cannot be represented as all-positive series. It is clear that, for nonzero s, G_0 has a maximum along S, corresponding to where the long-range Coulomb interaction is turned on, only to then decay. This means that the first derivative G_1 has a root, the second derivative has two roots, and so forth. Such nodes can only be achieved by the addition of terms that have opposite sign. The subtraction of two numbers to make a smaller number degrades the precision of the answer on a finite-precision machine.

Although it is not as elegant as the computation of the F_m, the G_m can be computed efficiently with enough precision for quantum chemistry purposes. In the remainder of this subsection, we will develop some algebra for computing the $G_m^{(n)}$, and in the next subsection we will discuss the actual steps in the evaluation with the precision of the result as a consideration.

We start by transforming the integrand of G_0, noting the symmetry with respect to $s^{1/2} \rightarrow -s^{1/2}$,

$$G_0(S,s) = \frac{\mathrm{e}^{-s}}{2}\int_{-1}^1 \mathrm{e}^{-Su^2}\cosh(2S^{1/2}s^{1/2}u)\,\mathrm{d}u \tag{15}$$

and then we insert the series expansion for cosh to obtain

$$G_0(S,s) = \mathrm{e}^{-s}\sum_{i=0}^{\infty}\left[\frac{(2S^{1/2}s^{1/2})^{2i}}{(2i)!}\int_0^1 u^{2i}\mathrm{e}^{-Su^2}\,\mathrm{d}u\right] =$$

$$\mathrm{e}^{-s}\sum_{i=0}^{\infty}\frac{2^{2i}S^i s^i}{(2i)!}\,F_i(S) \tag{16}$$

and finally, inserting the series in eq 13 for the F_i and rearranging the indices, we obtain an all-positive decaying series for G_0:

$$G_0(S,s) = \mathrm{e}^{-(S+s)}\sum_{i=0}^{\infty}\left[\left(\sum_{j=0}^{i}\frac{s^j}{j!}\right)\frac{(2S)^i}{(2i+1)!!}\right] \tag{17}$$

This can be simplified in terms of a family of functions $g_i^{(k)}$ that are related to the incomplete gamma function

$$G_0(S,s) = \sum_{i=0}^{\infty}\frac{(2i)!!}{(2i+1)!!}\,g_i^{(1)}(S)g_i^{(0)}(s)$$

$$g_i^{(k)}(x) = \left(-\frac{\partial}{\partial x}\right)^k\left[\frac{1}{i!}\int_x^\infty u^i\mathrm{e}^{-u}\,\mathrm{d}u\right] \tag{18}$$

We now obtain very easily

$$G_m^{(n)}(S,s) = \sum_{i=0}^{\infty}\frac{(2i)!!}{(2i+1)!!}\,g_i^{(m+1)}(S)g_i^{(n)}(s) \tag{19}$$

The primary advantages of eqs 10 and 11 is that the division by R has been absorbed into the integration, making it clear that the functions are finite in the $R \rightarrow 0$ limit, and indeed, the formulas in eqs 13 and 19 are evaluable at $R = 0$. However, we shall not want to build an infinitely large interpolation table over all S and s for the G_m. Yet for $S \approx s$, we would need such

a table even for large S. Also, the formula in eq 19 does degrade in precision as $S \approx s$ gets large.

The solution we seek is to return to the original form of the integral, and look at the large S limit, away from where this form is indeterminate:

$$\lim_{S\approx s\to\infty} G_0(S,s) = \lim_{R\approx r_0\to\infty} \left\{\frac{\pi^{1/2}}{2\varphi}\frac{1}{R}\frac{1}{2}\left[\mathrm{erf}(\varphi R + \varphi r_0) + \mathrm{erf}(\varphi R - \varphi r_0)\right]\right\} = \frac{\pi^{1/2}}{2}\frac{1}{S^{1/2}}h^{(0)}(S^{1/2} - s^{1/2})$$

$$h^{(k)}(x) = \left(-\frac{\partial}{\partial x}\right)^k \frac{1}{2}\left[1 + \mathrm{erf}(x)\right] \tag{20}$$

and then differentiate to obtain

$$\lim_{S\approx s\to\infty} G_m(S,s) = \frac{\pi^{1/2}}{2}\left(-\frac{\partial}{\partial S}\right)^m\left[\frac{1}{S^{1/2}}h^{(0)}(S^{1/2} - s^{1/2})\right] = \frac{\pi^{1/2}}{2^{m+1}}\left(\frac{-1}{S^{1/2}}\frac{\partial}{\partial S^{1/2}}\right)^m\left[\frac{1}{S^{1/2}}h^{(0)}(S^{1/2} - s^{1/2})\right] = \frac{\pi^{1/2}(2m-1)!!}{2^{m+1}}\left(\frac{1}{S}\right)^{m+1/2}\left[\sum_{k=0}^{m} a_{mk}h^{(k)}(S^{1/2} - s^{1/2})S^{k/2}\right] \tag{21}$$

The a_{mk} values are constant coefficients resulting from the algebra. We note that the a_{m0} values are exactly unity for all m, meaning that the leading $k = 0$ term of this expansion is the asymptotic form of F_m given in eq 14, multiplied by a function that starts as zero for $S \ll s$ and goes to unity at $S \gg s$. The remaining terms are Gaussian-like and produce the wiggles and nodes in the $S \approx s$ region. For any given S and s, we compute the difference between their square roots and use an interpolation table for the h_k, and then compute the sum. For a large magnitude of $S^{1/2} - s^{1/2}$, the h_k values all go very quickly to either zero or unity, meaning that we only need to interpolate over a region near zero.

3.3. Implementation Details. In constructing an interpolation table for the G_m, a greater number of the $G_m^{(n)}$ will need to be constructed at regularly spaced grid points. If we use 10×10-term interpolation to construct functions up to G_{12} during a calculation (up to f functions), we will need derivatives up to $G_{12+10}^{(10)}$ at the grid points. For this we use eq 19. First, the function

$$g_i^{(1)}(x) = \mathrm{e}^{-x}\frac{x^i}{i!} \tag{22}$$

is constructed for grid values of x and integers i, because it is the easiest. The maximum value of x necessary is the maximum value of S or s for the region over which direct interpolation is necessary, i.e., where eq 21 is not valid. We have found this maximum to be 150. For $S < 150$ and $s < 150$, summing up to $i = 500$ seems to be a sufficient number of terms in eq 19 for all $m \leq 22$ and $n \leq 10$ (i will always need to be much greater than S and s, and increasing m or n necessitates more terms). Then

$$g_i^{(0)}(x) = \sum_{j=0}^{i} g_j^{(1)}(x) \tag{23}$$

is used to construct $g_0^{(i)}$ over the same x and i. Finally,

$$g_i^{(k)}(x) = g_i^{(k-1)}(x) - g_{i-1}^{(k-1)}(x) \tag{24}$$

is used recursively to construct the higher $g_i^{(k)}$ over the same x and i, for k up to $22 + 1$; defining $g_i^{(k)}(x) = 0$ for $i < 0$ ensures self-consistency of eq 24. The recursive use of eq 24 causes a severe degradation in the precision of the higher $g_i^{(k)}$. Additionally, the summation in eq 19 also contains comparable terms of opposite sign, giving an unacceptably noisy result. For these reasons, we do all steps in 256-bit precision, using the GNU multiple-precision library;[60] the final $G_m^{(n)}$ values at each grid point are then stored as a 64-bit double precision number. Because of the large amount of time, memory, and disk resources required to compute the interpolation table entries, the final table is stored on disk (~50 Mb) as a permanent resource to a development version of the Q-Chem program package.[61] We judged that summing to $i = 500$ using 256-bit precision was sufficient on the basis of the fidelity of the final G_m for $m \leq 12$; determining the fidelity of the answer is discussed later.

Using 10×10-term interpolation with $m \leq 12$, the only open question is then one of grid spacing for the interpolation table. This could be better optimized, but that should be the subject of later work. We have found that 1/16-integer spacing is sufficient over the entire first quadrant of the (S,s) plane; the other quadrants correspond to imaginary values for physical quantities. For $S > 4$ or $s > 2$, eighth-integer spacing is sufficient. For $S > 10$ or $s > 5$, quarter-integer spacing is sufficient. For $S > 40$ or $s > 20$, half-integer spacing is sufficient. Again, we determined that the grid spacing was sufficient on the basis of the fidelity of the final G_m.

For $S > 70$ or $s > 150$, however, the cheaper formula in eq 21 is precise enough, and only one, one-dimensional interpolation table over a finite range for the h_k suffices for the rest of the first quadrant. We determined that the eq 21 is valid when its error relative to eq 19 is less than one part in 10^{14}. We use 10-term interpolation for the $h^{(k)}$ with 1/50-integer spacing over the domain $[-29, 29]$. The grid spacing was deemed to be sufficient on the basis of the fidelity of the final $h^{(k)}$ for $k \leq 12$. The domain was chosen, because outside of $[-29,29]$, the $h^{(k)}$ values are machine-zero ($<10^{-307}$), except for $h^{(0)}$ at 29, which has asymptoted to unity, to within machine precision. This domain is larger than necessary and needs to be optimized.

Now we comment on what is meant by the fidelity of a function value over an interpolated region. The grid spacing over a given region is deemed sufficiently tight if, for all points in that region that are located directly between the grid points (between two grid points for one dimension and centered between four grid points in two dimensions), interpolation from either/any of the nearest grid points yielded a relative difference of 10^{-14} or less in the function value. Near the nodes of the $m \neq 0$ or $k \neq 0$ functions, 14 digits of accuracy is not obtained, because the function value is getting very small, and it is being computed as the difference of numbers that are on the order of the function value away from the nodes. This is acceptable because we still obtain these values to the same absolute decimal place as the rest of the function, but these numbers are tiny. If the above manipulations had not been made, the most straightforward expressions give the G_m as differences between numbers that are orders of magnitude larger than the function value, even away from the nodes. We note that, for both the G_m and $h^{(k)}$, the high m or k cases present worst-case scenarios, demanding the tightest grid spacing over the largest domains.

Efficiency has not been the major concern of the present work, but even at present, the algorithm does not add substantial cost relative to the conventional Coulomb integrals. The G_m information that is generated is very primitive and sits below the generally more expensive building of angular harmonics and contractions.

4. Conclusion

We believe that this is the first time a straightforward cutoff has been applied to the Coulomb operator itself in a quantum mechanical context (rather than to the integrals), and the truncation region can be variably smoothed with our proposed attenuator. Concerning local correlation, optimization of the parameters in our attenuator have led us to a form of the truncated potential that is already familiar from classical dynamics, whereby the potential is truncated and shifted downward (and, in this case, smoothed); the reach of the inner range of this potential, over which the Coulomb repulsion is well-represented, can be easily and systematically extended in a smooth manner. This new tool will hopefully find use in both the study of correlation as well as the construction of efficient algorithms. In comparison with the popular erfc attenuator, we find that we obtain comparable results for dispersion-type interactions, and much better physics for shorter range correlations. This was shown to be important for covalent interactions and is likely to be important if a property such as an ionization energy or electron affinity is to be calculated. The use of Coulomb attenuation to truncate correlation is suitable for use in methods that yield smooth potential energy surfaces without risk of hysteresis. In this paper we have investigated only short-range correlation perturbatively. A useful variation on this theme would be to consider using the divided operator to solve for short-range correlations with a more accurate method and handle the long-range correlations by perturbation theory, as done in the work of Subotnik et al.[17] Finally, we have shown that the integral of our proposed attenuator can be computed stably over Gaussian basis functions.

Acknowledgment. The following people are thanked for helpful discussions on this subject: Peter Gill, Alex Sodt, Joseph Subotnik, and Albert Pan. We gratefully acknowledge funding from the Director of the Office of Basic Energy Sciences, Chemical Sciences Division of the U.S. Department of Energy, under Contract DE-AC03-76SF0098.

References and Notes

(1) Adamson, R. D.; Gill, P. M. W. *J. Mol. Struct. (THEOCHEM)* **1997**, *398*−*399*, 45.
(2) Pulay, P. *Chem. Phys. Lett.* **1983**, *100*, 151.
(3) Saebo, S.; Pulay, P. *Chem. Phys. Lett.* **1985**, *113*, 13.
(4) Pulay, P.; Saebo, S. *Theor. Chim. Acta* **1986**, *69*, 357.
(5) Saebo, S.; Pulay, P. *J. Chem. Phys.* **1987**, *86*, 914.
(6) Saebo, S.; Pulay, P. *Annu. Rev. Phys. Chem.* **1993**, *44*, 213.
(7) Maslen, P. E.; Head-Gordon, M. *Chem. Phys. Lett.* **1998**, 283, 102.
(8) Maslen, P. E.; Head-Gordon, M. *J. Chem. Phys.* **1998**, *109*, 7093.
(9) Schütz, M.; Hetzer, G.; Werner, H.-J. *J. Chem. Phys.* **1999**, *111*, 5691.
(10) Schütz, M.; Werner, H.-J. *Chem. Phys. Lett.* **2000**, 318, 370.
(11) Schütz, M. *J. Chem. Phys.* **2000**, *113*, 9986.
(12) Lee, M. S.; Maslen, P. E.; Head-Gordon, M. *J. Chem. Phys.* **2000**, *112*, 3592.
(13) Schütz, M.; Werner, H.-J. *J. Chem. Phys.* **2001**, *114*, 661.
(14) Schütz, M. *J. Chem. Phys.* **2002**, *116*, 8772.
(15) Werner, H.-J.; Manby, F. R.; Knowles, P. J. *J. Chem. Phys.* **2003**, *118*, 8149.
(16) Maslen, P. E.; Dutoi, A. D.; Lee, M. S.; Shao, Y.; Head-Gordon, M. *Mol. Phys.* **2005**, *103*, 425.
(17) Subotnik, J. E.; Sodt, A.; Head-Gordon, M. *J. Chem. Phys.* **2006**, *125*, 074116.
(18) Greengard, L.; Rokhlin, V. *J. Comput. Phys.* **1985**, *60*, 187.
(19) White, C. A.; Johnson, B. G.; Gill, P. M. W.; Head-Gordon, M. *Chem. Phys. Lett.* **1994**, *230*, 8.
(20) Russ, N.; Crawford, T. *J. Chem. Phys* **2004**, *121*, 691.
(21) Dombroski, J. P.; Taylor, S. W.; Gill, P. M. W. *J. Phys. Chem.* **1996**, *100*, 6272.
(22) Lee, A. M.; Taylor, S. W.; Dombroski, J. P.; Gill, P. M. W. *Phys. Rev. A* **1997**, *55*, 3233.
(23) Gill, P. M. W. *Chem. Phys. Lett.* **1997**, *270*, 193.
(24) Adamson, R. D.; Dombroski, J. P.; Gill, P. M. W. *Chem. Phys. Lett.* **1996**, *254*, 329.
(25) Panas, I. *Chem. Phys. Lett.* **1995**, *245*, 171.
(26) Panas, I.; Snis, A. *Theor. Chem. Acc.* **1997**, *97*, 232.
(27) Savin, A.; Flad, H.-J. *Int. J. Quantum Chem.* **1995**, *56*, 327.
(28) Leininger, T.; Stoll, H.; Werner, H.-J.; Savin, A. *Chem. Phys. Lett.* **1997**, *275*, 151.
(29) Toulouse, J.; Savin, A.; Flad, H.-J. *Int. J. Quantum Chem.* **2004**, *100*, 1047.
(30) Angyan, J. G.; Gerber, I. C.; Savin, A.; Toulouse, J. *Phys. Rev. A* **2005**, *72*, 012510.
(31) Gori-Giorgi, P.; Savin, A. *Phys. Rev. A* **2006**, *73*, 032506.
(32) Toulouse, J.; Savin, A. *J. Mol. Struct. (THEOCHEM)* **2006**, *762*, 147.
(33) Goll, E.; Werner, H.-J.; Stoll, H.; Leininger, T.; Gori-Giorgi, P.; Savin, A. *Chem. Phys.* **2006**, *329*, 276.
(34) Iikura, H.; Tsuneda, T.; Yanai, T.; Hirao, K. *J. Chem. Phys.* **2001**, *115*, 3540.
(35) Tawada, Y.; Tsuneda, T.; Yanagisawa, S.; Yanai, T.; Hirao, K. *J. Chem. Phys.* **2004**, *120*, 8425.
(36) Kamiya, M.; Sekino, H.; Tsuneda, T.; Hirao, K. *J. Chem. Phys.* **2005**, *122*, 234111.
(37) Chiba, M.; Tsuneda, T.; Hirao, K. *J. Chem. Phys.* **2006**, *124*, 144106.
(38) Sekino, H.; Maeda, Y.; Kamiya, M.; Hirao, K. *J. Chem. Phys.* **2007**, *126*, 014107.
(39) Tokura, S.; Yagi, K.; Tsuneda, T.; Hirao, K. *Chem. Phys. Lett.* **2007**, *436*, 30.
(40) Vydrov, O. A.; Heyd, J.; Krukau, A. V.; Scuseria, G. E. *J. Chem. Phys.* **2006**, *125*, 074106.
(41) Jacquemin, D.; Perpète, E. A.; Vydrov, O. A.; Scuseria, G. E.; Adamo, C. *J. Chem. Phys.* **2007**, *127*, 094102.
(42) Heyd, J.; Scuseria, G. E.; Ernzerhof, M. *J. Chem. Phys.* **2003**, *118*, 8207.
(43) Heyd, J.; Scuseria, G. E. *J. Chem. Phys.* **2004**, *121*, 1187.
(44) Krukau, A. V.; Vydrov, O. A.; Itzmaylov, A. F.; Scuseria, G. E. *J. Chem. Phys.* **2006**, *125*, 224106.
(45) Prodan, I. D.; Scuseria, G. E.; Martin, R. L. *Phys. Rev. B* **2007**, *76*, 033101.
(46) Batista, E. R.; Heyd, J.; Hennig, R. G.; Uberuaga, B. P.; Martin, R. L.; Scuseria, G. E.; Umrigar, C. J.; Wilkins, J. W. *Phys. Rev. B* **2006**, *74*, 121102(R).
(47) Peralta, J. E.; Heyd, J.; Scuseria, G. E. *Phys. Rev. B* **2006**, *74*, 073101.
(48) Barone, V.; Peralta, J. E.; Uddin, J.; Scuseria, G. E. *J. Chem. Phys.* **2006**, *124*, 024709.
(49) Gill, P. M. W.; Adamson, R. D.; Pople, J. A. *Mol. Phys.* **1996**, *88*, 1005.
(50) Yanai, T.; Tew, D. P.; Handy, N. C. *Chem. Phys. Lett.* **2004**, *393*, 51.
(51) Peach, M. G. J.; Cohen, A. J.; Tozer, D. J. *Phys. Chem. Chem. Phys.* **2006**, *8*, 4543.
(52) Cohen, A. J.; Mori-Sanchez, P.; Yang, W. *J. Chem. Phys.* **2007**, *126*, 191109.
(53) Jung, Y.; Sodt, A.; Gill, P. M. W.; Head-Gordon, M. *Proc. Natl. Acad. Sci. (U.S.A.)* **2005**, *102*, 6692.
(54) Jung, Y.; Lochan, R. C.; Dutoi, A. D.; Head-Gordon, M. *J. Chem. Phys.* **2004**, *121*, 9793.
(55) Lochan, R. C.; Jung, Y.; Head-Gordon, M. *J. Phys. Chem. A* **2005**, *109*, 7598.
(56) Gill, P. M. W.; Adamson, R. D. *Chem. Phys. Lett.* **1996**, *261*, 105.
(57) Adamson, R. D.; Dombroski, J. P.; Gill, P. M. W. *J. Comput. Chem.* **1999**, *20*, 921.
(58) Gill, P. M. W. *Adv. Quantum Chem.* **1994**, *25*, 141.
(59) Helgaker, T.; Taylor, P. R. In *Modern Electronic Structure Theory*; Yarkony, D. R., Ed.; World Scientific: River Edge, NJ, 1994; p 725.
(60) Granlund, T. *GNU MP: The GNU Multiple Precision Arithmetic Library 4.1.4*. GMP Web Page. http://www.swox.com/gmp.
(61) Shao, Y.; Molnar, L. F.; Jung, Y.; Kussmann, J.; Ochsenfeld, C.; Brown, S. T.; Gilbert, A. T. B.; Slipchenko, L. V.; Levchenko, S. V.; O'Neill, D. P.; DiStasio, R. A., Jr.; Lochan, R. C.; Wang, T.; Beran, G. J. O.; Besley, N. A.; Herbert, J. M.; Lin, C. Y.; Van Voorhis, T.; Chien, S. H.; Sodt, A.; Steele, R. P.; Rassolov, V. A.; Maslen, P. E.; Korambath, P.

P.; Adamson, R. D.; Austin, B.; Baker, J.; Byrd, E. F. C.; Dachsel, H.; Doerksen, R. J.; Dreuw, A.; Dunietz, B. D.; Dutoi, A. D.; Furlani, T. R.; Gwaltney, S. R.; Heyden, A.; Hirata, S.; Hsu, C.-P.; Kedziora, G.; Khalliulin, R. Z.; Klunzinger, P.; Lee, A. M.; Lee, M. S.; Liang, W.; Lotan, I.; Nair, N.; Peters, B.; Proynov, E. I.; Pieniazek, P. A.; Rhee, Y. M.; Ritchie, J.; Rosta, E.; Sherrill, C. D.; Simmonett, A. C.; Subotnik, J. E.; Woodcock, H. L., III; Zhang, W.; Bell, A. T.; Chakraborty, A. K.; Chipman, D. M.; Keil, F. J.; Warshel, A.; Hehre, W. J.; Schaefer, H. F., III; Kong, J.; Krylov, A. I.; Gill, P. M. W.; Head-Gordon, M. *Phys. Chem. Chem. Phys.* **2006**, *8*, 3172.